The Cracks Effect Analysis on In-Plane Diffusivity in Proton Exchange Membrane Fuel Cell Catalyst Layer by Lattice Boltzmann Method

Mingyang Yang, Song Yan, Aimin Du, and Sichuan Xu(✉)

School of Automotive Studies, Tongji University, 4800 Cao'an Road, Shanghai 201804, People's Republic of China
scxutj@163.com

Abstract. Crack is always considered as a kind of defect on a catalyst layer in a proton exchange membrane fuel cell (PEMFC), and its enhancement on mass transfer ability has always been ignored. In this work, the crack effect analysis on in-plane (IP) diffusivity on a catalyst layer is numerically evaluated by a D2Q9 lattice Boltzmann method (LBM). The effects on some key parameters like crack length, width, quantity and shape are carried out. The IP concentration distribution of crack CL shows deviation from the theoretical value, and this is because of the tortuosity caused by the CL cracks. The crack shape has almost no effect on the IP effective diffusivity, and the crack length shows a little bit more influence than the crack width and quantity. The crack ratio of the CL is the dominant effect on the IP mass diffusivity enhancement, and the lower the CL porosity is, the higher this enhancement achieve.

Keywords: Proton exchange membrane fuel cell · Catalyst layer · Crack

1 Introduction

Cracks formation on CLs during the operational process mostly bring unexpected defects, mostly regarded as degradations and failures. These defects occur at the crack formation reign, including crack propagation to membrane pinholes, increasing in-plane (IP) resistance (R_{IP}) of CLs, formation of flooding areas and catalyst degradation [1]. Some operation conditions are prone to crack initiation, such as freeze-thaw (F-T) cycles [2], dry-wet cycles [3], cyclic loadings [4], and ionomer degradation [5]. However, some work has claimed the mass transfer enhancement by the cracks on CL [6–8].

In this work, to understand the crack effect on the PEMFC catalyst layer IP diffusivity, a lattice Boltzmann method D2Q9 model was employed. The normalized concentration of air in the cracked CL was acquired, and the effective diffusivity of the complex crack zone was calculated by the flux field. This model was validated by the analytical result and shows relatively high accuracy. The effects on some key parameters like crack length, crack width, crack quantity and crack shape were carried out.

H. Sun et al. (Eds.): WHTC 2023, SPPHY 393, pp. 141–150, 2024.
https://doi.org/10.1007/978-981-99-8631-6_16

2 Random Crack Domain Regeneration

A processed base crack regeneration method was employed to obtain a computational field. The details of this method were described in our previous work [9]. The circle cracks were introduced in this simulation because some former work showed a significant enhancement in mass transfer using this CL structure [10]. The non-crack area (NCA), the intact porous catalyst layer, and the crack area (CA), the chapped crack, were defined in the computational domain. These two different regions have different properties on diffusion.

3 Physical and Mathematical Model

3.1 Physical Description

In a cracked CL, the effective diffusivity D^{eff} is determined by the NCA phase and CA phase properties. Although the exact value of the D^{eff} is hard to estimate, its value is in the range of D_{CA} and D_{NCA}.

$$D^{eff} \in [D_{CA}, D_{NCA}] \tag{1}$$

The NCA and CA phase in this research are porous CL structure and air, respectively. The mass diffusivity $D^{p}_{O_2}$ in the nanostructure is reported to be sensitive to the porous CL structure due to the effect of Knudsen diffusion [11], which is shown as

$$\frac{1}{D^{p}_{O_2}} = \frac{1}{D_{Kn}} + \frac{1}{D_{O_2}} \tag{2}$$

The D_{O_2} is oxygen diffusivity is equal to the D_{NCA}, and the D_{Kn} is Knudsen diffusivity. These values can be calculated as

$$D_{O_2} = 0.22 \times 10^{-4} \frac{(T/293.2\text{K})^{1.5}}{p/1\text{ atm}} \tag{3}$$

$$D_{Kn} = 4850 d_p \sqrt{\frac{T}{M}} \tag{4}$$

where p is the absolute pressure in atm, and is set to 2.5 atm (absolute pressure). T is temperature in K, and is set to 353 K. M is the molecular weight of oxygen in g/mol, and is set to 32 g/mol. d_p is the characteristic pore size in cm [11]. The mean d_p is used in the modeling and an empirical correlation of the mean d_p is given as

$$d_p = 140.50\varepsilon^2 + 68.35\varepsilon + 38.08 \tag{5}$$

To obtain the diffusivity D_{NCA} in the NCA media, a Bruggeman-like power law is employed as [11]

$$D_{NCA} = 1.07\varepsilon^{1.75} \times D^{p}_{O_2}$$

Combining Eq. (2)–(6), the diffusivity of NCA media at different porosities are acquired. In this research, the porosity is in 0.25~0.45.

3.2 Governing Equations

A 2D model is employed for the IP mass transfer analysis. Figure 1 illustrates the computational domain of a cracked CL, and the governing equations for mass diffusion can be expressed as following equations,

$$\frac{\partial C}{\partial t} = D_{NCA}\left(\frac{\partial^2 C}{\partial x^2} + \frac{\partial^2 C}{\partial y^2}\right) \tag{7a}$$

$$\frac{\partial C}{\partial t} = D_{CA}\left(\frac{\partial^2 C}{\partial x^2} + \frac{\partial^2 C}{\partial y^2}\right) \tag{7b}$$

The boundary conditions are described as

$$\begin{cases} C = C_1, \ y = L, 0 \le x \le L \\ C = C_2, \ y = 0, 0 \le x \le L \\ f_{1,5,8}|_{x=0} = f_{1,5,8}|_{x=L} \\ f_{3,6,7}|_{x=L} = f_{3,6,7}|_{x=0} \end{cases} \tag{8}$$

where C is the concentration. The top and bottom boundary are maintained at C_1 and C_2 using famous Zou-he boundary conditions [12]. To ensure stability of the numerical method, a small difference which is 0.01 is set between these two boundaries. The periodic boundary is set at the left and right boundaries as previous works [13].

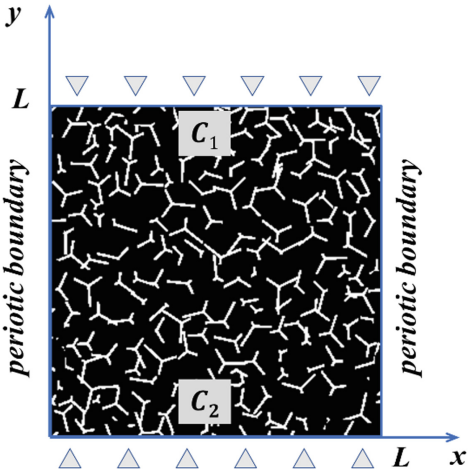

Fig. 1 Computational domain of cracked CL.

3.3 2D LBM Model Description

In this research, a two-dimensional (2D) LBM single relaxation time (SRT) model is employed to solve the mass transfer phenomenon in different phases. The density distribution function g_α evolution equation for a two-dimensional nine-speed (D2Q9) LBM

in both NCA and CA can be given as,

$$g_\alpha(\boldsymbol{r}+\boldsymbol{e}_\alpha\delta_t, t+\delta_t) - g_\alpha(\boldsymbol{r}, t) = -\frac{1}{\tau}\left[g_\alpha(\boldsymbol{r}, t) - g_\alpha^{eq}(\boldsymbol{r}, t)\right] \tag{9}$$

where $\boldsymbol{r}$ is the position vector, t is the real time, δ_t is the iteration time step, ${g_\alpha}^{eq}$ is the equilibrium distribution function of the evolution equation.

The gases phase in the NCA is assumed to be static, because the *Peclet Number* (*Pe*) in the porous structure is relatively low. Thus, the ${g_\alpha}^{eq}$ shows as [14].

$$g^{eq}(x,t) = \begin{cases} 0, & \mathrm{i} = 0 \\ \frac{1}{6}C, & \mathrm{i} = 1\text{ - }4 \\ \frac{1}{12}C, & \mathrm{i} = 5\text{ - }8 \end{cases} \tag{10}$$

The velocity vector $\boldsymbol{e}_i$ for D2Q9 scheme is

$$\boldsymbol{e}_i = \begin{cases} (0,0) & i = 0 \\ \boldsymbol{e}\left(\cos\left[\frac{\pi}{2}(i-1)\right], \sin\left[\frac{\pi}{2}(i-1)\right]\right) & i = 1,2,3,4 \\ \sqrt{2}\boldsymbol{e}\left(\cos\left[\frac{\pi}{2}(i-1)\right], \sin\left[\frac{\pi}{2}(i-1)\right]\right) & \sqrt{2}i = 5,6,7,8 \end{cases} \tag{11}$$

and τ is the dimensionless relaxation time for NCA and CA, which is determined by the diffusivity coefficient [15],

$$\tau_{CA} = \frac{3}{2}\frac{D_{CA}}{(\rho c)_{CA}\cdot c^2\delta_t} + 0.5 \tag{12}$$

and

$$\tau_{NCA} = \frac{3}{2}\frac{D_{NCA}}{(\rho c)_{NCA}\cdot c^2\delta_t} + 0.5 \tag{13}$$

where c is a pseudo sound speed, D_{CA} and D_{NCA} are the diffusivity coefficient in crack area and non-cracked area, respectively. To ensure the continuities of the flux and density distribution functions at the interface of different phases, the ρc is set to 1 in this model [16]. Then the calculation of macroscopic quantities of the density and flux can be obtained by

$$T = \sum_i f_i, \tag{14}$$

$$J = \left(\sum_i c_i f_i\right)\frac{\tau - 0.5}{\tau}. \tag{15}$$

At the end of each computational loop, the effective diffusivity coefficient D^{eff} can be obtained by Fick's law [17, 18]:

$$D^{eff} = \frac{L_x \int J dA}{(C_2 - C_1)\int dA}. \tag{17}$$

where C_2 and C_1 are the boundary values of inlet and outlet boundaries, respectively. L_x is the distance between these two boundaries, and A is the computational width of the domain.

The normalized effective diffusivity coefficient D^n is defined as [19],

$$D^n = D^{eff}/D_{NCA}. \tag{18}$$

The D_{NCA} is equal to the D^{O_2}, which is the oxygen diffusivity in bulk. This normalized method makes the crack effect obviously on the diffusivity change of the CLs.

4 Results and Discussion

4.1 Model Validation

Two typical structures, the "parallel" and the "series" model which are introduced in the previous work are used to validate the LBM model [20]. In the model validation section, the CR is set to 0.5. The D_{CA}/D_{NCA} value is set to 1–1000. Meanwhile, the domain side length effect is also taken into consideration which is set from 300 to 5000 μm at the resolution of 10 μm. The model validation result is shown in Fig. 2. When the domain side length is small, the error value is big, and the error is sensitive to the ratio between two conductivity values. To balance the computational consumption and an error less than 1%, the domain side length is set to 3000 μm, and the conductivity ratio is limited at 1:100. In another word, the representative element volume (REV) in this case is 3000 μm × 3000 μm.

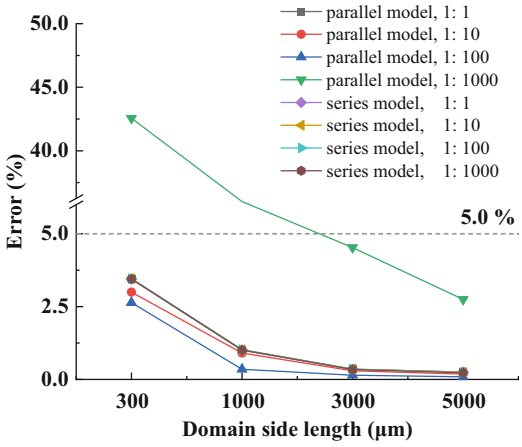

Fig. 2. Comparison between model prediction value and theoretical value.

4.2 IP Effective Transfer Properties Influenced by Cracks

Normalized Concentration with Diffusion Time. To evaluate the effect of diffusion time on normalized concentration in the crack area, a bunch of simulations are designed. The porosity of NCA is 0.3, and five different crack quantities are selected from 20 to 180. The triangle crack with 25 μm crack width are reconstructed, and every crack arm length is random from 0 to 200 μm. As shown in Fig. 3, the average temperature at each coordinate with 180 cracks is higher than that of 20 cracks. The D_{CA} is significant than the D_{NCA}, thus a higher *CR* is good for mass transport in the CLs. After 15e5 lattice steps, the computing converges, but none of the concentration reaches the theoretical linear line. This is because the existence of cracks changes the real tortuosity of the mass

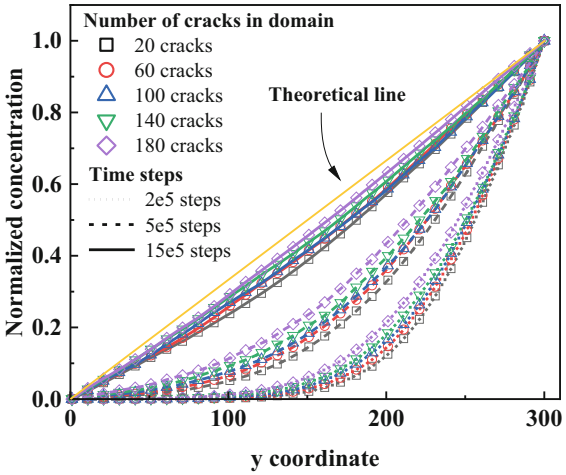

Fig. 3. The normalized concentration distribution with different time steps.

transfer. Furthermore, the more crack quantity, the farther the concentration deviates from the theoretical value.

Normalized Concentration with Crack Shape. To evaluate the effect of crack shape on the on normalized concentration in the crack area, three kinds of domains with different crack shape, which are linear cracks, circle cracks and triangle cracks were employed. The porosity of NCA is 0.3, and the *CR* were set to 0.15 ± 0.05. The triangle cracks case shows a little higher normalized concentration than that of linear crack and circle crack cases. However, when the calculation converges, all three cases shows similar normalized concentration distribution. In addition, the deviation of the computational value from the theoretical value is caused by the cracks affecting the tortuosity of the computational domain (Fig. 4).

Crack Ratio Effect on Diffusivity. To understand the effect of crack ratio on effective diffusivity, the relationship between crack ratio and normalized diffusivity was carried out. The NCA porosity is set to 0.2 and the D_{NCA}/D_{bulk} is 0.04111. Different crack width, length and quantity cases are carried out. Meanwhile, the parallel model and series model are also used as the upper and lower limit of the normalized diffusivity. With the CR increase from 0 to 0.15, the normalized diffusivity of crack width case, crack length case and crack quantity case increase from 0.0411 to 0.0682, 0.0780 and 0.0866, respectively. Thus, the crack length shows the highest influence on the IP mass transfer enhancement. The computational model result is between the parallel model and series model results (Fig. 5).

NCA Porosity Effect on Diffusivity. A lower porosity will cause a lower D_{NCA}, and the relationship between these two parameters is shown in Eqs. (2)–(6). When the porosities are 0.2, 0.3, 0.4 and 0.5, the D_{NCA}/D_{bulk} are 0.0411, 0.089, 0.1579 and 0.2452, respectively. And the simulation is carried out for these four cases. Result shows, with the crack ratio increase from 0 to 0.17, the IP diffusivity enhancements of 0.2, 0.3, 0.4

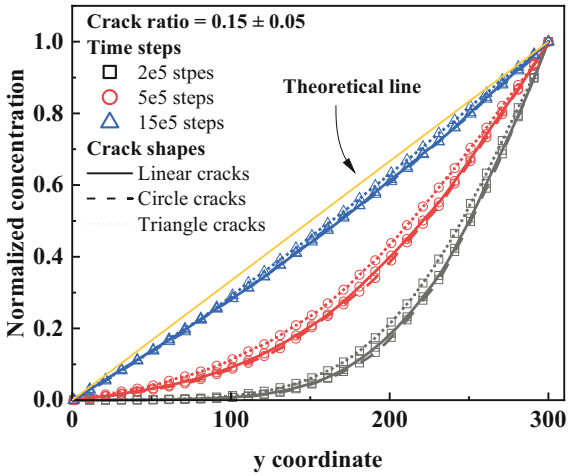

Fig. 4. The normalized concentration distribution of different crack shapes.

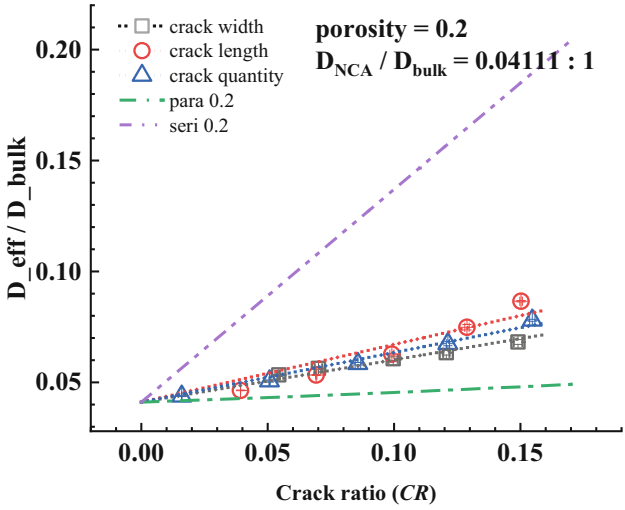

Fig. 5. Diffusivity change caused by crack ratio change.

and 0.5 porosity cases are about 96.93%, 63.86%, 43.40% and 30.08%, respectively. Considering the relative low porosity of CL structure, this enhancement shows great potential to enhance the IP mass transportation of oxygen phase and water vapor phase (Fig. 6).

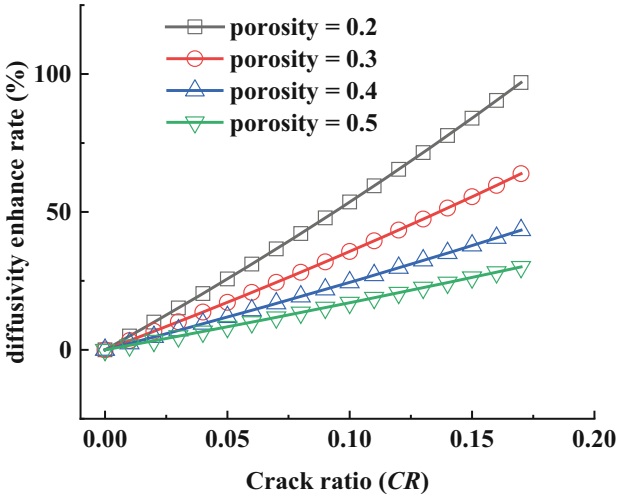

Fig. 6. Diffusivity change caused by NCA porosity change.

5 Conclusions

In order to understand the crack effect on the PEMFC catalyst layer IP diffusivity, a lattice Boltzmann method D2Q9 model was employed in this research. The normalized concentration of mass transport was acquired, and the effective diffusivity of the complex crack zone was calculated by the flux result. The following conclusions were mainly obtained:

1. The LBM model shows good accuracy when the diffusivity ratio is bigger than 1: 100. The error is below 5% when the domain size is 300 μm × 300 μm, and the error is below 0.5% when the domain size is 3000 μm × 3000 μm.
2. For a triangle crack, the crack length shows a little bit more influence than the crack width and quantity. However, comparing to the parameter including length, width, quantity and shape, the *CR* plays the dominant role in the diffusivity enhancing.
3. Considering the relative low porosity of CL structure, there is a great potential to enhance the IP mass transportation of oxygen phase and water vapor phase by design the cracked morphology.

References

1. Kundu, S., Fowler, M.W., Simon, L.C., Grot, S.: Morphological features (defects) in fuel cell membrane electrode assemblies. J. Power. Sources **157**(2), 650–656 (2006)
2. Lee, S.-Y., Kim, H.-J., Cho, E., Lee, K.-S., Lim, T.-H., Hwang, I.C., et al.: Performance degradation and microstructure changes in freeze–thaw cycling for PEMFC MEAs with various initial microstructures. Int. J. Hydrogen Energy **35**(23), 12888–12896 (2010)
3. Uchiyama, T,. Kumei, H., Yoshida, T.: Catalyst layer cracks by buckling deformation of membrane electrode assemblies under humidity cycles and mitigation methods. J. Power Sources **238**, 403–412 (2013)

4. Kai, Y., Kitayama, Y., Omiya, M., Uchiyama, T., Kato, M.: Crack formation in membrane electrode assembly under static and cyclic loadings. J. Fuel Cell Sci. Technol. **10**(2) (2013)
5. Singh, Y., Orfino, F.P., Dutta, M., Kjeang, E.: 3D failure analysis of pure mechanical and pure chemical degradation in fuel cell membranes. J. Electrochem. Soc. **164**(13), F1331–F1341 (2017)
6. Vengatesan, S., Panha, K., Fowler, M.W., Yuan, X.-Z., Wang, H.: Membrane electrode assembly degradation under idle conditions via unsymmetrical reactant relative humidity cycling. J. Power Sour. **207**, 101–110 (2012)
7. Yin, Y., Li, R., Bai, F., Zhu, W., Qin, Y., Chang, Y., et al.: Ionomer migration within PEMFC catalyst layers induced by humidity changes. Electrochem. Commun. 109 (2019)
8. Park, C.H., Lee, S.Y., Hwang, D.S., Shin, D.W., Cho, D.H., Lee, K.H., et al.: Nanocrack-regulated self-humidifying membranes. Nature **532**(7600), 480–483 (2016)
9. Yang, M., Yan, S., Du, A., Liu, J., Xu, S.: Effect of micro-cracks on the in-plane electronic conductivity of proton exchange membrane fuel cell catalyst layers based on lattice Boltzmann method. Int. J. Hydrogen Energy (2022)
10. Hou, Y., Deng, H., Pan, F., Chen, W., Du, Q., Jiao, K.: Pore-scale investigation of catalyst layer ingredient and structure effect in proton exchange membrane fuel cell. Appl. Energy **253**, 113561 (2019)
11. Zheng, W., Kim, S.H.: The effects of catalyst layer microstructure and water saturation on the effective diffusivity in PEMFC. J. Electrochem. Soc. **165**(7), F468–F478 (2018)
12. Zou, Q., He, X.: On pressure and velocity boundary conditions for the lattice Boltzmann BGK model. Phys. Fluids **9**(6), 1591–1598 (1997)
13. Chen, L., Kang, Q., Tao, W.: Pore-scale numerical study of multiphase reactive transport processes in cathode catalyst layers of proton exchange membrane fuel cells. Int. J. Hydrogen Energy **46**(24), 13283–13297 (2021)
14. Wang, M., He, J., Yu, J., Pan, N.: Lattice Boltzmann modeling of the effective thermal conductivity for fibrous materials. Int. J. Therm. Sci. **46**(9), 848–855 (2007)
15. Qu, Z.G., Fu, Y.D., Liu, Y., Zhou, L.: Approach for predicting effective thermal conductivity of aerogel materials through a modified lattice Boltzmann method. Appl. Therm. Eng. **132**, 730–739 (2018)
16. Wang, M., Wang, J., Pan, N., Chen, S.: Mesoscopic predictions of the effective thermal conductivity for microscale random porous media. Phys. Rev. E Stat. Nonlin. Soft Matter Phys. **75**(3 Pt 2), 036702 (2007)
17. Hu, B., Wang, J.G.: Fractal microstructure effects on effective gas diffusivity of a nanoporous medium based on pore-scale numerical simulations with lattice Boltzmann method. Phys. Rev. E. **104**(6–2), 065304 (2021)
18. Lange, K.J., Sui, P.-C., Djilalia, N. : Pore scale simulation of transport and electrochemical reactions in reconstructed PEMFC catalyst layers (2010)
19. García-Salaberri, P.A., Zenyuk, I.V., Shum, A.D., Hwang, G., Vera, M., Weber, A.Z., et al.: Analysis of representative elementary volume and through-plane regional characteristics of carbon-fiber papers: diffusivity, permeability and electrical/thermal conductivity. Int. J. Mass Transf. **127**, 687–703 (2018)
20. Tuncer, E., Gubański, S.M., Nettelblad, B.: Dielectric relaxation in dielectric mixtures: Application of the finite element method and its comparison with dielectric mixture formulas. J. Appl. Phys. **89**(12), 8092–8100 (2001)